Dynamics of the Kv1.2 Voltage-Gated K$^+$ Channel in a Membrane Environment

Vishwanath Jogini and Benoît Roux
Institute of Molecular Pediatric Sciences, Gordon Center for Integrative Science, The University of Chicago, Chicago, Illinois

ABSTRACT   All-atom molecular dynamics simulations are used to better understand the dynamic environment experienced by the Kv1.2 channel in a lipid membrane. The structure of the channel is stable during the trajectories. The pore domain keeps a well-defined conformation, whereas the voltage-sensing domains undergo important lateral fluctuations, consistent with their modular nature. A channel-like region at the center of the S1–S4 helical bundle fills rapidly with water, reminiscent of the concept of high-dielectric aqueous crevices. The first two arginines along S4 (R294 and R297) adopt an interfacial position where they interact favorably with water and the lipid headgroups. The following two arginines (R300 and R303) interact predominantly with water and E226 in S2. Despite the absence of a structurally permanent gating pore formed by protein residues and surrounding the S4 helix, as traditionally pictured, the charged residues are located in a favorable environment and are not extensively exposed to the membrane nonpolar region. Continuum electrostatic computations indicate that the transmembrane potential sensed by the charged residues in the voltage sensor varies abruptly over the outer half of the membrane in the arginine-rich region of S4; thus, the voltage gradient or membrane electric field is "focused". Interactions of basic residues with the lipid headgroups at the intracellular membrane-solution interface reduce the membrane thickness near the channel, resulting in an increased transmembrane field.

INTRODUCTION

Voltage-dependent K$^+$ (Kv) channels alter their conformation in response to changes in the membrane potential, thereby allowing or blocking the conduction of ions (1). They are formed by four subunits surrounding a central aqueous pore for K$^+$ permeation. Each subunit comprises six transmembrane segments, S1–S6, the first four, S1–S4, constituting the voltage-sensor domain, and the last two, S5 and S6, forming the pore (2). Four highly conserved arginine residues along S4 have been identified as predominantly responsible for the gating charge controlling the voltage activation of the channel (3,4). Upon membrane depolarization, the voltage sensor in each subunit undergoes a transition from a resting to an activated state, which is followed by a concerted transition leading to the opening of the pore (5–8).

Structural information is a prerequisite to understanding Kv channels. The crystal structure of Kv1.2 has provided the first atomic-resolution view of a eukaryotic Kv channel (9). The x-ray structure is in broad accord with what had been previously deduced, on the basis of a wide range of structural, functional, and biophysical experiments, about the homologous *Shaker* K$^+$ channel in its activated open state (10,11), thereby strengthening the consensus about the structure of Kv channels. Specifically, the voltage sensor is formed by four antiparallel transmembrane α-helices, S1–S4 (packed in a counterclockwise fashion seen from the extracellular side), and the S4 helix of a subunit is within proximity of S5 from the adjacent subunit (nearest in the clockwise direction) (10).

The lack of extensive interaction between the voltage sensor and the pore domain is striking. About 66% of the molecular surface of the transmembrane region of each voltage sensor (S1–S4) is exposed to lipids, with the rest covered by the pore domain (S5 and S6); ~25% of S4 is exposed to lipids. The discovery of voltage-sensor-like domains in two unrelated proteins that lack a pore domain (12–14) unambiguously established the concept of the S1–S4 helical bundle as an independent functional module.

Although the x-ray structure of Kv1.2 provides important information, additional considerations are necessary to picture the channel in the dynamic environment of a fully hydrated phospholipid membrane. Furthermore, many of the side chains in the transmembrane region of the voltage sensor were not resolved in the crystal structure, and the computations can shed light on some of the key details that remain uncertain. In particular, the position and orientation of the charged arginine side chains along S4 are controversial. Long et al. (9) proposed that the outermost two arginines along S4 project into the nonpolar hydrocarbon core of the membrane, whereas a more traditional view would have them directed toward the bulk water phase. The orientation of those side chains is poorly defined in the crystal structure (their B-factor is ~160 Å^2) and the crystal environment lacks a dynamic membrane in the fluid state. As one probes deeper into the mechanism of Kv channels, it is essential to ascertain the configurations of the voltage sensor and its charged side chains in a realistic environment.

Molecular dynamics simulations based on detailed atomic models can help resolve some of those issues and provide a better view of the channel in its dynamic environment. Previous simulations of the Kv1.2 channel (15) and of the

isolated voltage sensor of the KvAP channel (16,17), provide a wealth of detail about these systems. Our goal is to further the exploration of the structure and dynamics of the Kv1.2 channel in a fully hydrated lipid membrane, and, more specifically, to characterize the coupling of the charged residues in the voltage sensor to the transmembrane potential. Our aim with these calculations is to complement the information that is currently available from experiments as well as from previous simulation studies, and to contribute to the understanding of Kv channels. The atomic model and the computational methodology are described in the next section. In the following sections, the results are reported and then discussed. The article concludes with a brief summary of the main results.

THEORY AND METHOD

Structural models of Kv channels

Because the x-ray structure of the Kv1.2 channel is incomplete, it is necessary to model the missing elements by exploiting all available information. A critical examination of previous models, constructed before the x-ray structure of Kv1.2, shows that it is possible to make best use of all available experimental information from homologous channels with some confidence. The various models are compared with x-ray structures in Fig. 1. The pore domain of an early model of *Shaker* by Laine et al. (10), generated before the x-ray structure of the KvAP channel (18), was based on the x-ray structure of the MthK channel (19). A subsequent model of *Shaker* by Chanda et al. (20) incorporated structural elements from the x-ray structure of the KvAP channel (i.e., the pore domain and the voltage-sensor module) (18). Though there are clearly some structural differences, the main structural features of the latest model from Chanda et al. (20) are in excellent agreement with the x-ray structure of the Kv1.2 channel. As predicted, the

voltage sensor is formed by a bundle of four antiparallel transmembrane helices, S1–S4, each with their N- and C-terminal ends exposed, alternately, to the intra- and extracellular solution. The transmembrane helices forming the voltage sensor are packed counterclockwise (21). The first arginine residue of S4 (R362 in *Shaker* and R294 in Kv1.2) is not far from the C-terminus of S5 (F416 and A419 in *Shaker* or F348 and A351 in Kv1.2) and the voltage sensor makes contact with the adjacent subunit in the clockwise direction (10). The approximate models captured the main topological features of the Kv1.2 structure; ~75–80% of the total molecular surface area of S4 is covered by S1–S3 and by the contact with the S5 helix in the pore domain. Only the remaining 20–25% is exposed to lipids. In comparison, the fraction of the surface of S4 exposed to lipid was ~12% in the *Shaker* models by Laine et al. (10) and ~22% in the model by Chanda et al. (20). The z-position of the Cα of the first arginine in S4 (R294 in Kv1.2 and R362 in *Shaker*) is at 13.7 Å from the center of the bilayer in Kv1.2 (9), and at 11.1 Å and 12.5 Å, respectively, in the *Shaker* models by Laine et al. (10) and Chanda et al. (20).

The excellent accord between the x-ray structure and results from numerous functional and biophysical experiments considerably strengthens and solidifies the growing consensus about voltage-gated K$^+$ channels. It also increases confidence in the modeling based on a wide range of biophysical data. For the current simulations of the Kv1.2 channel in a lipid membrane, only the transmembrane part of the channel comprising the segment S1–S6 was included in the model. For the sake of simplicity, the N-terminal T1 domain (residues 1–150), the C-terminus (residues 422–576), and the β-aldo-keto reductase domain were not included. Residues L151 and T421 are set to be the zwitterionic NH$_3^+$ and COO$^-$ termini in each protein subunit. Furthermore, the S1–S2 and S3–S4 linkers were truncated to shorter helix turns similar to those in the voltage sensor of the KvAP channel. For the S1–S2 linker, residues 185–214 were not included. For the S3–S4 linker, residues 282–286 were deleted, in accord with experimental data indicating that such deletions are not detrimental to the channel function (22). The system described here is somewhat less ambitious than the model simulated by Treptow and Tarek (15), which included the T1 domain as well as the long interhelical loops that are not resolved in the x-ray structure of Kv1.2. Because this investigation is focused on the transmembrane domain and
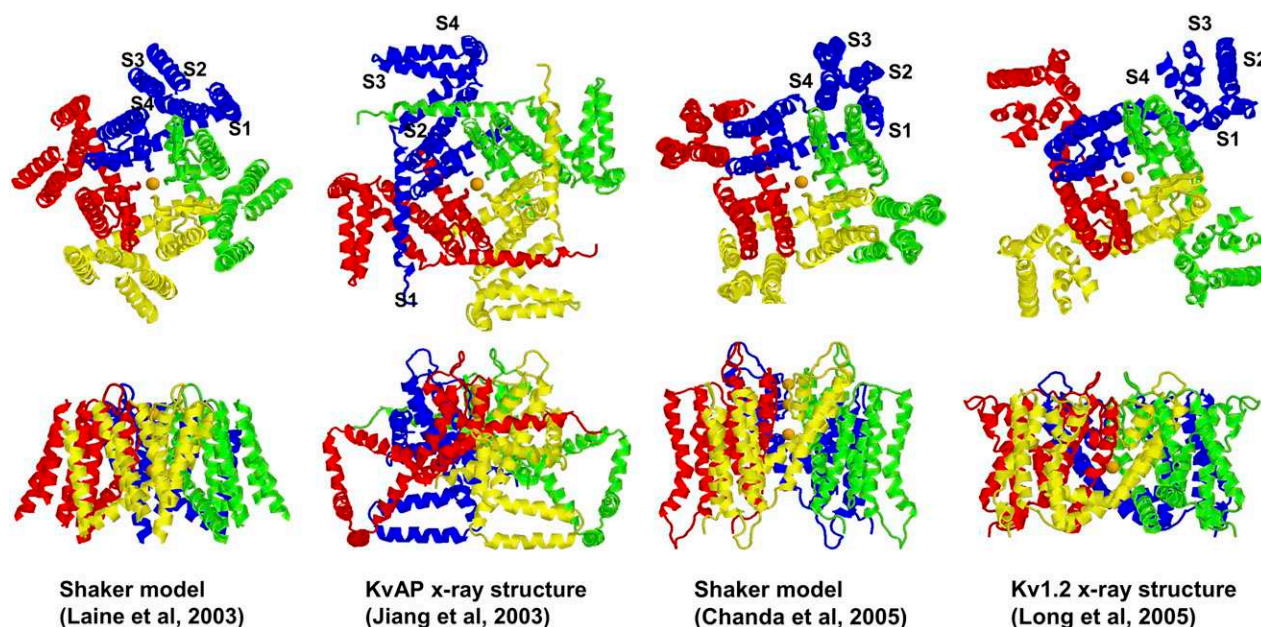

FIGURE 1 Comparison of the models of *Shaker* from Laine et al. (10) and Chanda et al. (20) with the x-ray structure of the KvAP channel (18) and the x-ray structure of the Kv1.2 channel (9).

the charged residues of the voltage sensor, we chose to not include structural elements that increase computational cost and add uncertainty to the model.

The model was constructed using structural information from the crystal structure of the Kv1.2 channel (PDB code 2A79) and from the isolated voltage sensor of the KvAP channel (PDB code 1QRS). Because of the moderate resolution of the diffraction data, most of the side chains of the voltage sensor in 2A79 are not identified, and the segments S1 and S3 are modeled as polyalanine helices called UNK1 and UNK2, respectively. Structural alignments and mutagenesis functional data were used to assign the residues forming the UNK1 and UNK2 segments. The strategy is similar to that used previously to model the *Shaker* channel (11). Briefly, amino acid positions along S1 and S2 identified as being functionally tolerant to tryptophan substitutions were used to match the lipid-exposed positions along UNK1 (23–26). In particular, nine positions along UNK1 are lipid-exposed and can be matched to the 13 Trp-tolerant residues in *Shaker* (23,24). Nevertheless, the uncertainty about S1 is not detrimental to the model, since channel function is generally tolerant to mutations in S1, suggesting that a perfect alignment of the (mainly nonpolar) residues of this segment is probably not critical (23,24). To assign the unidentified residues of S3, the Mg^{2+} binding site engineered in the *eag* (ether-à-go-go) Kv channel between D278 (in S2) and D327 (in S3) was used (21). By analogy, this result implies proximity of the corresponding residues I230 (in S2) and F267 (in S3) in the Kv1.2 channel. Three positions (6, 10, and 14) along the UNK2 segment corresponding to S3 are near I230 in S2. To assign these positions to specific residues in the sequence of Kv1.2, the structure of the isolated voltage sensor of the KvAP channel was used (18). The backbone Cα atoms of residues 101–105 and 115–128 in KvAP were structurally aligned onto the Kv1.2 structure. According to this alignment, position 10 along the UNK2 segment most closely matched G101 of the KvAP channel, corresponding to F267 in the Kv1.2 channel.

The four outermost arginine residues along the S4 segment are R294, R297, R300, and R303. Based on the x-ray structure of the Kv1.2 channel, the two outermost arginines (R294 and R297) are positioned at the periphery of the protein (27). After orienting the channel structure relative to a bilayer centered at $z = 0$, the two side chains are located near the membrane-solution interface with their Cαs around $z = 15$ Å and 13.5 Å, respectively. The side chain of R294 is near the interface with the guanidinium group centered on CZ at $z = 15.6$ Å, whereas R297, constructed with its CZ at $z = 11.5$ Å, points directly into the hydrocarbon core of the membrane. To explore the stability of alternate side-chain rotamers for R297 in the S4 segment, the simulations were carried out using the side-chain conformation from the x-ray structure for two of the four channel subunits, and using an optimized rotamer from SCWRL (28) for the other two subunits. The algorithm in SCWRL searches for optimal rotamers using a backbone-dependent library of side chains. According to SCWRL, the side chain of R297 should point away from the membrane toward the aqueous solution. With its CZ at $z =$ 17.6 Å, R297 is oriented to be well hydrated. This is in general accord with the optimal rotamer for an arginine side chain along an α-helix pointing roughly in the direction of the N-terminus (29).

Molecular dynamics simulations

The molecular dynamics (MD) simulation system represents an atomic model of the Kv1.2 channel embedded in a dipalmitoylphosphatidylcholine (DPPC) bilayer surrounded by an aqueous salt solution of 100 mM KCl. The atomic model comprises the Kv1.2 tetramer of 944 amino acids (15,084 atoms), 176 DPPC molecules (81 in the top layer and 95 in the bottom layer), and 12,859 water molecules and 3 K^+ ions in the pore. To make the entire system electrically neutral, 23 K^+ and 22 Cl^- were added in the bulk solution, yielding a concentration of 100 mM KCl at zero transmembrane potential. The total number of atoms in the entire system is 76,826. The protein-membrane system was constructed from preequilibrated and prehydrated lipid molecules, according to a protocol described previously (30–32). The center of the bilayer is at $z = 0$. The channel is oriented perpendicular to the membrane plane such that the pore is along the z axis. Two simulations with different configurations of the ions in the pore, $[S_0,S_2,S_4]$ and $[S_1,S_3,S_{cav}]$, were generated. A picture of the simulation system is shown in Fig. 2.

All the calculations were performed using the biomolecular simulation program CHARMM, version c32a2 (33). The all-atom potential energy function PARAM27 for protein (34) and phospholipids (35) was used. The TIP3P potential function was used for water (36). The Lennard-Jones parameters for K^+ and Cl^-, adjusted to yield the experimental solvation free energy in bulk water, were used (37). Periodic boundary conditions are applied to simulate a multilayer system of membrane extending in the xy plane. Electrostatic interactions in the periodic system are calculated according to the particle mesh Ewald algorithm (38) and short-range nonbonded interactions are truncated at 10 Å. The dimensions of the periodic system are $100 \times 100 \times 80$ Å^3. During simulation, the z dimension of the unitary cell is allowed to vary according to the constant pressure and temperature thermodynamic ensemble (39), whereas its xy dimensions are fixed. The temperature was set to 315 K, above the phase-transition temperature of pure DPPC membranes (n.b., the presence of a protein impurity also lowers the transition temperature relative to that of pure membrane) (40). The SHAKE algorithm was used to fix the bond lengths involving hydrogen atoms (41) with an integration time step of 2 fs. As in previous simulations of proteins with explicit membrane bilayers (30–32), the initial configuration of the system was first relaxed with Langevin dynamics at constant volume in the presence of harmonic constraints applied to the channel atoms to avoid any spurious disruption of the protein structure. The two systems were carefully relaxed and equilibrated, and each was followed by 20 ns of production MD.
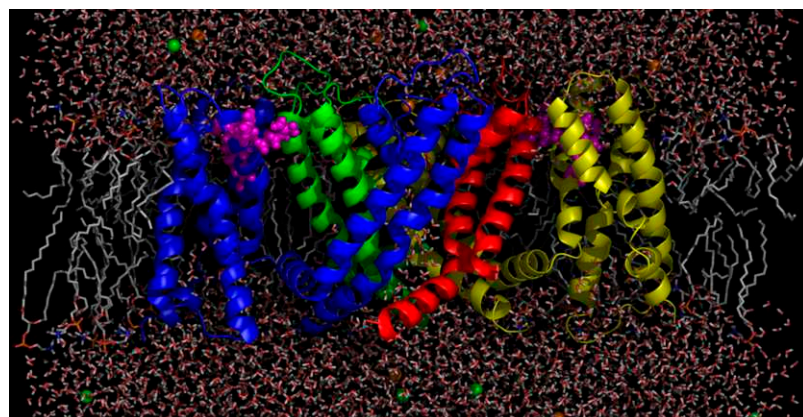

FIGURE 2 Molecular representation of the Kv1.2 channel embedded in DPPC membrane solvated by a 100-mM KCl aqueous solution. K^+ ions (*brown*) and Cl^- ions (*green*) are shown as spheres, and arginine gating charges (*magenta*) are shown in ball and stick format. For clarity, the voltage sensor of one subunit (*red*) and the lipids in front of the channel are not shown.

Continuum electrostatic calculations

The membrane voltage profile was calculated using a continuum electro-static approximation based on the Poisson-Boltzmann equation modified to account for the effect of the transmembrane voltage (PB-V) (42,43)

$$\nabla \cdot [\varepsilon(\mathbf{r})\nabla\phi_{mp}(\mathbf{r})] - \bar{\kappa}^2(\mathbf{r})[\phi_{mp}(\mathbf{r}) - \Theta(\mathbf{r})] = 0, \quad (1)$$

where $\varepsilon(\mathbf{r})$ and $\kappa(\mathbf{r})$ are the space-dependent dielectric coefficient and Debye-Hückel ionic screening factor, respectively, and $\Theta(\mathbf{r})$ is a Heaviside step function equal to 0 on one side of the membrane and 1 on the other side (42,43). PB-V is a linear continuum electrostatic theory based on a Green's-function decomposition of the total free energy. According to Eq. 1, the atomic charges of the proteins are turned off for this calculation (no source term on the righthand side). Mathematically, $\phi_{mp}(\mathbf{r})$ corresponds to the dimensionless fraction of the applied transmembrane potential V_{mp} at the point $\mathbf{r} = (x,y,z)$. It varies between 0 (on the intracellular side) and 1 (on the extracellular side). All results concerning the transmembrane voltage are calculated from ϕ_{mp} using Eq. 1.

The conformation-dependent contribution of the transmembrane potential to the total free energy of the protein takes the form (42)

$$\Delta G_{mp}(\mathbf{R}^{(s)}; V_{mp}) = V_{mp} \sum_i q_i[\phi_{mp}(\mathbf{r}_i^{(s)})], \quad (2)$$

where $\mathbf{r}^{(s)} \equiv \left\{\mathbf{r}_1^{(s)}, \mathbf{r}_2^{(s)}, \ldots, \mathbf{r}_n^{(s)}\right\}$ denotes all the protein coordinates in conformational state "s", q_i is the ith protein charge, V_{mp} is the transmembrane potential, and $\phi_{mp}(\mathbf{r})$ corresponds to the dimensionless fraction of the transmembrane potential at the point $\mathbf{r}$ defined by the PB-V equation (42). In Eq. 2, the sum over the index i runs over all the atoms of the channel. From the solution to the PB-V equation for a given configuration of the channel, the free-energy contribution (normalized by V_{mp}) for each charged residue in the voltage sensor was calculated via Eq. 2 by restricting the sum over i to the atoms of that residue. It should be noted that although the configurations of the open state are taken from a trajectory generated with no transmembrane potential, they can be used in conjunction with Eqs. 1 and 2 to calculate $\phi_{mp}(\mathbf{r})$ and ΔG_{mp}. For a given residue, each configuration taken from the trajectory provides four independent values, one for each subunit of the channel. The z-position assigned to the charged residues was calculated as an average weighted over the atomic charges of the residues.

The PB-V calculations were performed using the PBEQ module of the biomolecular simulation program CHARMM (33), version c32a2. The PB-V equation was solved numerically with a finite-difference relaxation algorithm for an ensemble of 20 instantaneous configurations (1/ns) taken from the MD trajectory (n.b., these trajectories were generated with no transmembrane potential). A cubic grid 120 Å wide with 1 grid point/Å was used. Previous tests have shown that this grid spacing yields sufficient accuracy. In the PB-V calculations, the channel, with its voltage sensors, the two K^+ ions and water molecules in the selectivity filter, and the DPPC membrane were represented explicitly with atomic details in their instantaneous configuration. The remaining ions and water molecules were removed, and their effect was represented by a continuum with a dielectric constant of 80 and a salt concentration of 100 mM (i.e., the membrane in the PB-V calculations is set by the explicit lipids). The internal dielectric constant of the protein and lipids was set to 2. The dielectric boundaries were constructed with a reentrant algorithm using the set of Born atomic radii optimized for protein and nucleic acids.

RESULTS

The simulated system is shown in Fig. 2. The channel and the membrane remain stable throughout the two 20-ns simulations (after equilibration). The overall picture emerging from the two simulations is similar. Salt bridges are formed between neighboring charged residues in S2, S3, and S4 within the voltage-sensor domain, and between S4 and S5 from the adjacent subunit. In addition, water molecules rapidly hydrate the charged residues of the protein and strong interactions between the arginine residues of S4 with the lipid headgroups are observed. In the following text, we first examine the structural fluctuations of the channel. The key interactions pertaining to the stability and dynamics of the voltage sensor are then described and discussed. Finally, the environment of the four outermost arginines of S4 and their coupling to the transmembrane potential is characterized.

Structural fluctuations of the channel and voltage-sensor module

The average root mean-square deviation (RMSD) of the channel backbone relative to the initial structure is 4.5 Å for the tetramer. The RMSD of the pore domain is <2.0 Å and the selectivity filter is very stable throughout the simulations, with a RMSD of 0.98 Å. The magnitude of the lateral fluctuations of the voltage-sensing domains is large, on the order of 5–6 Å, whereas the RMSD of the individual voltage-sensing domains is only ~3 Å, indicative of their structural stability. A superposition of instantaneous configurations of the voltage sensor domain is shown in Fig. 3. The pore domain appears as a fairly stable structural unit, whereas the S1–S4 module undergoes obvious lateral whole-body motions within the membrane. The individual helices fluctuate, though the overall packing of the voltage sensor is maintained.

Intersubunit salt bridges between the side chains of R297 and D352 near the extracellular end of S5 from the adjacent subunit form spontaneously during the simulation. An optimal rotamer for R297, determined by SCWRL (28), already positions this side chain to favorably interact with D352 (keeping the backbone as in the x-ray structure). The interaction occurs transiently over the length of the simulation, fluctuating over periods of 3–5 ns. This behavior is observed for all four subunits. At the end of the simulation, R297 from two of the four subunits and R294 from one of the subunits form a salt bridge with D352 on the pore domain. The lipids and D352 compete to interact with R294.

The dynamic voltage sensor

Configurations and hydration of the arginines of S4

To characterize the environment of the gating residues of S4, the time evolution of the z-position of the four outermost arginines, as well as the fluctuating number of water molecules, carbon atoms from the lipid acyl chains, and headgroups surrounding the side chains, were monitored. The results for the two 20-ns MD trajectories are shown in Fig. 4. To ascertain the configuration of R297, two different initial rotameric states were considered; for two of the four channel subunits, the rotamer of R297 was kept unchanged
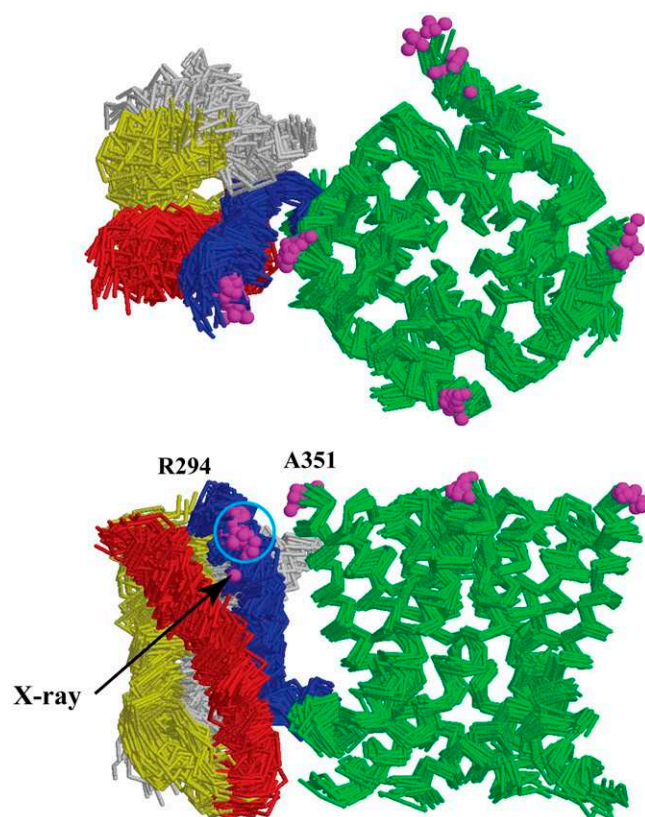
FIGURE 3 Fluctuations of the voltage-sensor module. The pore domain (*green*) is oriented with respect to the initial structure at an interval of 1 ns and the voltage-sensor modules from the four subunits are superimposed on each other. The voltage sensor comprises S1 (*white*), S2 (*yellow*), S3 (*red*), and S4 (*blue*). The C_β atoms of R294 and A351 are represented as magenta-colored spheres. The arrow indicates the initial position of R294.

from the crystal structure, whereas for the other two subunits, an optimal rotameric state, determined using the program SCWRL (28), was used. The time evolution during the trajectories shows that the side chains started in the x-ray orientation indeed have their CZ deeper in the membrane than the optimal rotamer from SCRWL, but move up rapidly. Whether or not SCWRL provides the right answer for a membrane protein, the procedure provides an opportunity to examine the stability of different starting configurations of the arginines of S4 for the simulations. In fact, within ~5 ns, the *z*-position of the side chain from the four subunits becomes indistinguishable and displays similar extended conformations. The x-ray side chains, which are not surrounded by water initially, start to become hydrated after ~3 ns, while most of the direct contacts with lipid acyl chains are lost in a period of ~5 ns. R294 adopts a more markedly interfacial position, retaining one or two direct contacts with the lipid chains over the entire simulation period. Neither R294 nor R297 penetrates into the central hydrocarbon core of the membrane (extending along the *z* axis in the ± 12 Å range).

Aqueous crevices

Water rapidly diffuses from the intracellular and extracellular sides to fill any crevices within the S1–S4 helical bundle, spontaneously forming a stable hourglass-shaped aqueous region interrupted at the center of the membrane (just below R303). All the charged residues of the voltage sensor become well solvated. R294 and R297, which are located at the membrane-solution interface, are solvated by around six water molecules on average. R300 and R303, which are located inside the crevice accessible from the extracellular side, are also well solvated; there are about six to nine water molecules around R300 and R303 on average (the time evolution of the hydration numbers is shown in Fig. 4). The aqueous crevices associated with the voltage sensors are visible in Fig. 2 (also see Fig. 8 *A* below).

Salt bridges within the voltage sensor

A number of specific salt-bridge interactions form spontaneously within the voltage-sensor domain. A salt bridge between R303 in S4 and E226 in S2 remains stable in three of the four subunits. Interactions between R300 and E226 are also observed, though they appear to be more transient, partly because water and lipids compete with E226 to interact with R300. Deeper within the voltage sensor, K306 forms salt bridges with E236 in S2, and with D259 in S3. These interactions were previously identified experimentally using second-site charge-reversal mutations in the homologous *Shaker* channel (44–46), where they correspond to E283 (in S2) with R368 and R371 (in S4), and K374 (in S4) with E293 (in S2) and D316 (in S3).

Interactions with the lipids

Monitoring the number of headgroups surrounding the arginines of S4 as a function of time shows that the interactions develop early on during both simulations (Fig. 4). At the end of the 20-ns trajectory, R294 and R297 of all four subunits have established salt bridges with the lipid headgroups. In two subunits, R294 interacts with two, or even three, lipids simultaneously. Interactions involving R300 and R303 are also observed, though they are short-lived and appear transiently; in one subunit, the side chain of R303, which normally forms a strong salt bridge with E226 in S2, shifts upward toward the extracellular side to interact with a lipid from the outer leaflet of the bilayer. At the intracellular end of S4, the side chain of R309 also forms a stable and long-lasting interaction with the lipids of the inner leaflet. K306, near the center of the membrane, does not come in contact with lipid headgroups and remains in stable interaction with E236 and D259. A typical configuration of S4 interacting with negatively charged residues and lipids in the upper and lower leaflets of the bilayer is shown in Fig. 5. Further examination also reveals that pairing of interfacial basic residues with the phosphate group is actually quite
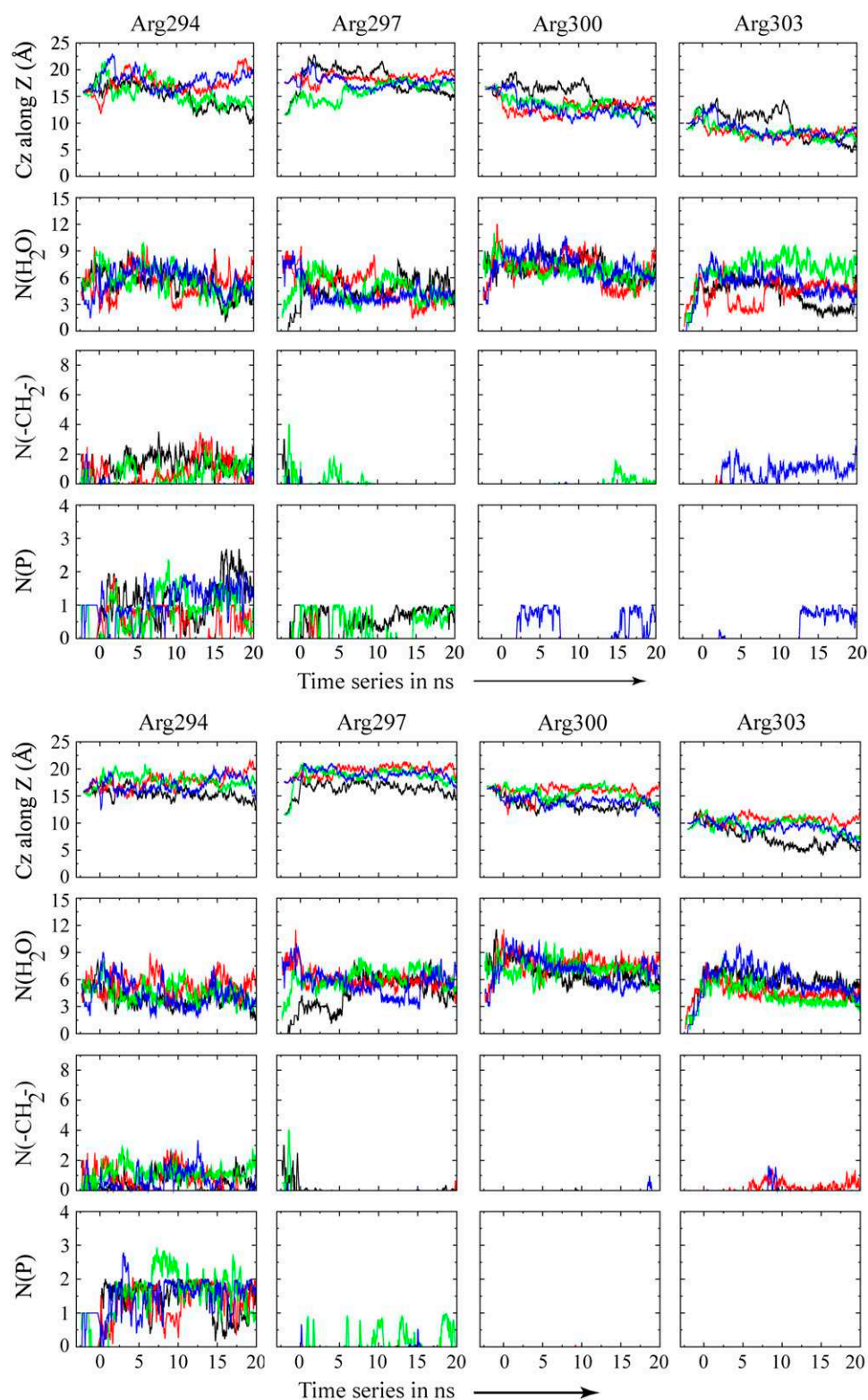
FIGURE 4 (*Upper*) MD simulation 1. (*Lower*) MD simulation 2. Environment around charged arginines on the S4 helix. The first panel shows the position of the guanidinium moiety along the *z*-axis, where the hydrophobic core of the lipid is extended from -12.5 to $+12.5$ Å. The second panel shows the number of water molecules 4 Å around the guanidinium moiety. The third panel shows the number of acyl chains 4 Å around the guanidinium moiety. The fourth panel shows the number of phosphates 4 Å around the guanidinium moiety. All graphs are plotted with a running average of 2 for times below 0 ns on the timescale and 50 for the rest of the simulation. Each subunit is represented with a different color.

common. It is observed for R294, R297, and R309 along the S4 segment, but also for R163 at the intracellular end of S1; K312, K322, and K326 in the S4–S5 linker; and R354 near the extracellular end of S5. The position of those residues is highlighted in Fig. 6. It is observed that the lipid headgroups are systematically pulled-in by the basic residues on the intracellular side and that the membrane is thinner near the channel by $\sim$5 Å.
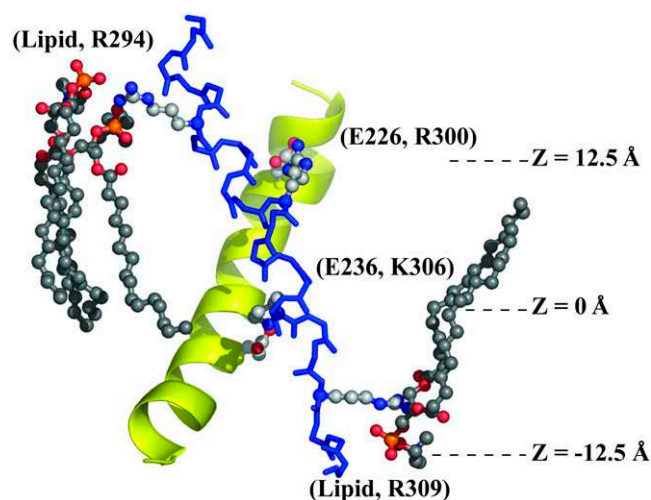
FIGURE 5 Schematic representation of countercharges near particular residues along the S4 segment. Three sets of salt bridges are depicted at three different positions relative to the membrane bilayer. All the side chains and lipids are shown in CPK. Only the S2 and S4 helices of the voltage sensor are shown.

Coupling to the transmembrane potential

To first examine the validity of the continuum approximation to describe the transmembrane voltage, a comparison was made with the simulations from Sachs et al. (47), which achieved a physically realistic transmembrane potential using explicit Nernst-Planck ion concentrations within a dual bilayer system. The voltage profile across a pure DPPC bilayer was calculated using the PB-V equation from an instantaneous configuration taken from the 50-ns MD trajectory of Klauda et al. (48). The results from the PB-V equation (normalized by V_{mp}) are shown in Fig. 7. The profile calculated from the PB-V equation is remarkably similar to the potential profile calculated with explicit Nernst-Planck ion

concentrations (47). This comparison confirms that the continuum electrostatic approximation underlying the PB-V theory is valid for the purpose of characterizing the coupling to a transmembrane voltage.

The results from the PB-V theory calculated with Eqs. 1 and 2 are shown in Fig. 8 C (normalized by V_{mp}), together with the density profile of the main components of the system shown in Fig. 8 B. The voltage profiles across a pure DPPC bilayer (dotted line) and along the central pore of the tetrameric channel (solid line) are also plotted for comparison. The two outermost arginines, R294 and R297, are positioned near the membrane-solution interface, at ~80% of the transmembrane potential. Deep in the center of the voltage sensor, E226 in S2 and R303, the fourth arginine along S4, are involved in a salt-bridge interaction resting at ~40% of the transmembrane voltage. The fifth charge along S4, K306, rests near the intracellular side, at ~10% of the transmembrane voltage. The first four arginine residues in S4 are located in the region where the potential varies from ~40% to 80% of the total voltage.

DISCUSSION

The two 20-ns simulations help delineate key features of a Kv channel with its voltage-sensor domains in the activated (''up'') conformation in the dynamic environment of a fully hydrated membrane. The tetrameric channel structure is stable throughout the simulations (Fig. 2), though the magnitude of the lateral fluctuations of the voltage-sensor domain is on the order of 5–6 Å (Fig. 3). Vertical fluctuations (along the z axis) of the voltage sensor relative to the pore domain are on the order of 3–4 Å. Intramolecular subunit-to-subunit distances display large variations. For example, the instantaneous distances between the backbone Cα of V295 in S4 (corresponding to V363 in Shaker) from adjacent
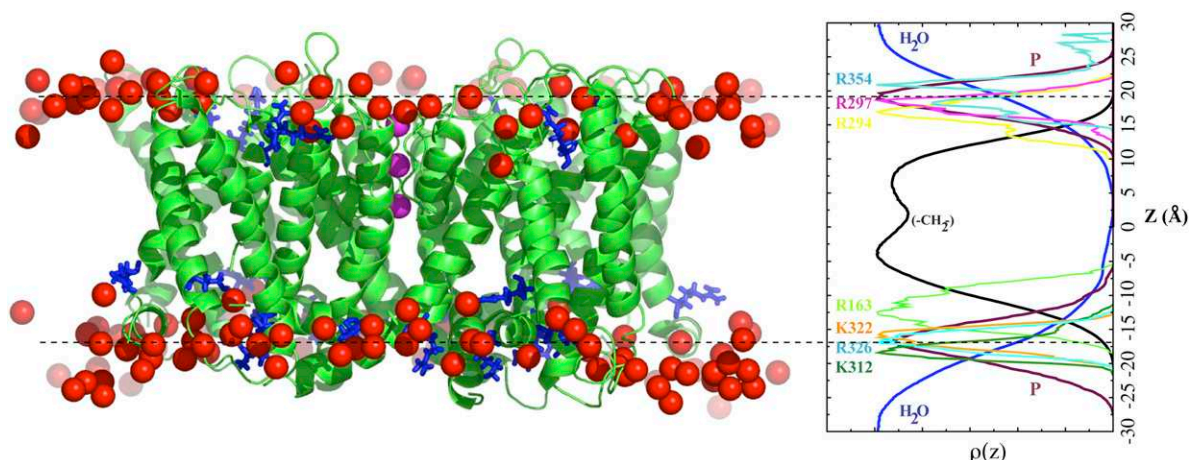

FIGURE 6 (Left) Basic residues are observed to interact directly with the phosphate group of the lipids: R163 at the intracellular end of S1; R294, R297, and R309 along the S4 segment; K312, K322, and R326 in the S4-S5 linker; and R354 near the extracellular end of S5. (Right) Density profile of the simulated system along the z axis. The membrane surface on the extracellular side is flat, but it is curved inward on the intracellular side.
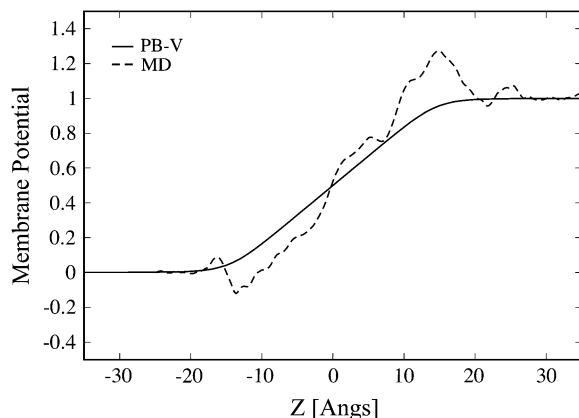
FIGURE 7 Comparison of the voltage profile across a pure DPPC bilayer, calculated from an instantaneous configuration taken from the 50-ns MD trajectory of Klauda et al. (48) using the PB-V equation (42) (*solid line*), with the potential profile calculated from explicit Nernst-Planck ion concentrations with a double bilayer system by Sachs et al. (47) (*dashed line*). The latter was obtained by subtracting the result with asymmetric and symmetric ion concentrations in Fig. 2a of Sachs et al. (47).

subunits yield a broad distribution centered around 49 Å and ~10 Å wide, i.e., instantaneous distances are spread out from 44 Å to 54 Å, and excursions as large as ~8 Å from the mean could occur ~2% of the time assuming a normal distribution. The magnitude of the vertical and lateral fluctuations has important implications for the interpretation of experiments aimed at estimating conformational changes by tethering fluorescent (49) or chemical probes (50,51) to

various parts of the voltage sensor. For instance, short distances tend to be weighted more heavily in fluorescence because the Förster energy-transfer rate varies like the inverse sixth power of the donor-acceptor distance (52), leading to apparent small motions. On the other hand, irreversible binding of avidin to biotin could capture the voltage sensor during a large excursion away from the dominant conformation in trapping experiments with biotinylated channels (51).

Consistent with the modular nature of the voltage sensor, only a small number of specific interactions with the pore domain of Kv channels have been identified experimentally (10,53–55). In particular, a high-affinity intersubunit His-His Zn^{2+} metal bridge was engineered in *Shaker* between R362 in S4 and A419 in S5 (10); the binding of Zn^{2+} greatly stabilizes the channel in the open activated state. In the x-ray structure of Kv1.2, the corresponding residues R294 and A351 are relatively distant from one another with a $C\beta$-$C\beta$ distance of 13.7 Å; the backbone of S4 would need to translate by at least ~5 Å to allow the formation of the bridge. Despite the large lateral fluctuations displayed by the voltage sensor during MD, a stable His-His metal bridge would require a net displacement of S4. The implications of these observations are unclear and would need to be further investigated.

Traditionally, in the ''sliding helix'' or ''helical screw'' models of voltage gating, it was assumed that S4 was moving inside a hydrophilic ''gating pore'' formed by protein residues, where it would be stabilized by water and salt-bridge interactions and sequestered from the surrounding lipids (56,57). This view was challenged by the paddle model of
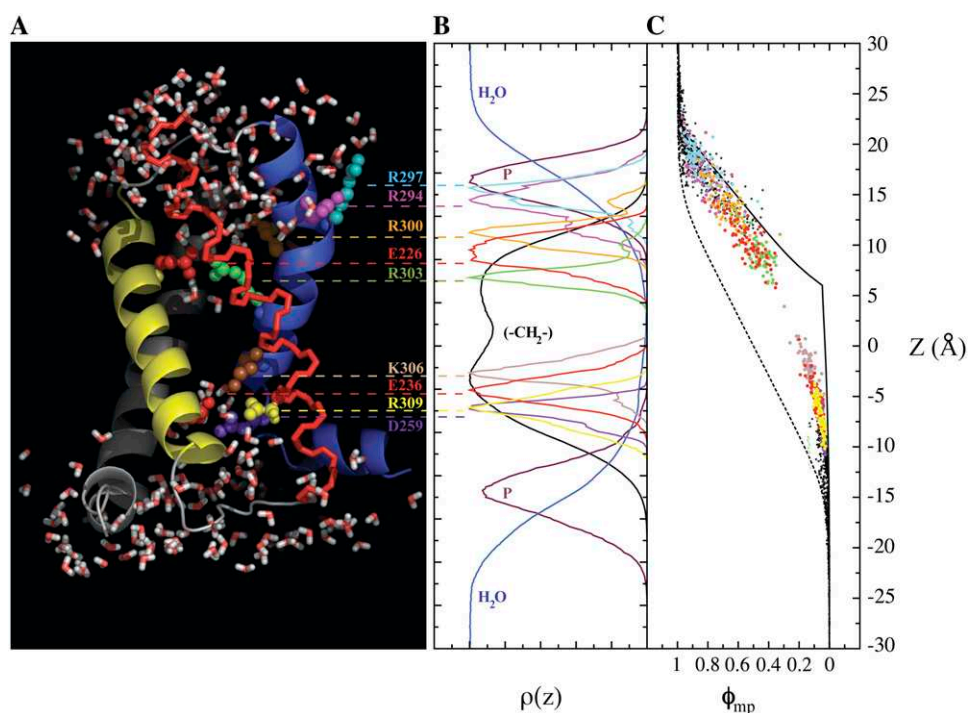

FIGURE 8 Organization of the charged residues in the voltage sensor and its relationship to the transmembrane potential profile calculated from the PB-V equation (42). (*A*) View of the aqueous crevices that develop rapidly during the simulation. (*B*) Density profile of the main component of the system along the membrane z axis, including the water, hydrocarbon chains, phosphate groups, and the most important charged residues of the voltage sensor. (*C*) Transmembrane potential sensed by the charged residues in the voltage sensor as a function of their average position along the z axis; included are NH_3^+–L154, E157, R163, E183, D220, E226, E236, R240, K247, D259, E273, E276, K277, E279, D280, R294, R297, R300, R303, K306, R309, and H310.

channel gating, which proposed that the charged arginines of S4 were directly exposed to the membrane (51). The x-ray structure of the Kv1.2 channel shows that S4 is not completely surrounded by protein, which led to the suggestion that the outermost two arginines along S4 might be projecting into the nonpolar hydrocarbon core of the membrane, consistent with the paddle model (9). However, even models of the *Shaker* channel shown in Fig. 1 indicated that S4 had to be partly exposed to lipids, by ~12% in the model of Laine et al. (10) and ~22% in the model of Chanda et al. (20) compared to ~20–25% for the x-ray structure of Kv1.2. By taking the membrane environment into account, MD simulations make it possible to go beyond such simple considerations based on static structures to assess the orientation of those side chains. The time evolution of the system in both trajectories shows that the first and second arginine (R294 and R297) rapidly adopt an interfacial location (including the side chains initiated in the x-ray conformation pointing into the lipid hydrocarbon), where they are located in a dynamic environment providing favorable polar interactions with water and lipids. This suggests that the orientation of the two outermost arginine side chains may have been affected by the lack of a fluid membrane in the crystal environment. The third and fourth arginines of S4 are also rapidly hydrated and become involved in stabilizing salt-bridge interactions with residues in S2. Consequently, all the charged residues of the voltage sensor find an energetically favorable environment where they are well hydrated and paired with acidic side chains and/ or lipid headgroups. More specifically, all charged side chains along S4 located within the bounds of the hydrocarbon core of the membrane (e.g., R300, R303, and K306) are turned toward the S1–S3 helices, where they interact with acidic residues. Despite the lack of a gating pore surrounding S4 in the traditional sense, no charged residue is extensively exposed to the hydrocarbon chains of the lipids. Effectively, all the charged residues implicated in voltage sensing are located in an energetically favorable environment, i.e., in a ''dynamic gating pore''.

A striking feature of these simulations is the high propensity for direct pairing of some arginine side chains with the lipid phosphodiester. As illustrated in Fig. 5, the vertical location of all the charged residues along S4 that are not directly stabilized by acidic residues in S2 or S3 matches the average structure of the bilayer, both at the extracellular (R294 and R297) and intracellular (R309) membrane-solution interface. By virtue of their position relative to the channel, the lipid headgroups provide favorable interactions with the charges in S4 that complement the S1–S3 segments; the charged residues of the S1–S3 segments interact with the charged residues of S4 that are within the membrane, whereas the lipid headgroups interact with those that are at the membrane interface (see Figs. 5 and 8 *B*). The presence of important lipid interactions is also consistent with recent results showing that, to function normally, the KvAP channel

requires the specific presence of lipids with a negatively charged phosphodiester (58). This could be indicative of specific residue-lipid interactions. There are other cases where direct lipid-channel interactions have been noted, e.g., anionic lipids are critical for the function of the KcsA channel (59).

As shown in Fig. 6, pairing with the lipid headgroups is actually not limited to the arginines along S4 (R294, R297, and R309), but is observed for many of the basic residues located near the membrane-solution interface, e.g., R163 at the intracellular end of S1, K312, K322, and R326 in the S4-S5 linker, and R354 near the extracellular end of S5. The high propensity of basic residues interacting with the lipid headgroup is generally consistent with the concept of interfacial basic residues ''snorkeling'' to the membrane surface (60). In the system described here, the interactions contribute to shift the intracellular membrane-solution interface (by ~5 Å). This renders the membrane thinner near the channel (Fig. 6), which in turn has an impact on the transmembrane field (see below). Given the high propensity of such interactions, it is perhaps not surprising that Kv channels inserted into a membrane lacking a negatively charged phosphodiester appear to be unable to function normally, as recently reported (58). The charge pairing might be greatly enhanced by the high local concentration of phosphate groups within the microenvironment of the membrane-solution interface (~3 M) and the proximity of the low-dielectric hydrocarbon membrane region. Near a nonpolar interface, the interaction of an arginine with a lipid headgroup is stronger and less shielded than if the charge pairing occurred in bulk solution. In vacuum, bare interaction between one arginine side chain and a lipid phosphate group is on the order of –100 kcal/mol. In aqueous solution, this interaction is much reduced due to dielectric shielding, but this reduction is not as effective near a nonpolar interface. The effective interaction between one arginine side chain and a lipid phosphate group in water and near a nonpolar interface were estimated using continuum electrostatics. In a continuum representing water with a dielectric constant of 80, the effective interaction is ~–5.5 kcal/mol. In a continuum dielectric representing water near the interface of a nonpolar slab 25 Å thick with a dielectric constant of 2, it is ~–12.3 kcal/mol. The increase is consistent with the fact that charge-charge interactions are much less shielded near a low dielectric slab, even if the charged pair remains in the high-dielectric water.

Water molecules diffuse rapidly and move into a channel-like region at the center of the S1–S4 helical bundle. As shown in Figs. 2, 4, and 8 *A*, water fills the small crevices above and below R303, forming an hourglass-shaped aqueous region. Very similar hydration structures have been reported in simulations of the Kv1.2 channel (15) and of the isolated voltage sensor of the KvAP channel (16,17), suggesting that the result is likely to be robust. The existence of an aqueous channel-like region at the center of the voltage sensor has been inferred by mutations in S4 that enabled the rapid conduction of ions in the inactivated (''down'') state

(61,62). For example, conduction of H^+ through the voltage sensor is not normally observed in the case of the wild-type channel, but the R371H is sufficient to allow H^+ conduction in *Shaker* (R303 in Kv1.2). The hourglass-shaped aqueous region going through the voltage sensor and connecting the extracellular and intracellular sides is interrupted just below R303 (Fig. 8 *A*). Similar observations have been made based on simulations of the KvAP voltage sensor (17). Although the interrupted water chain near R303 is in qualitative accord with experimental results, previous studies on other ''proton wires'' (63–65) suggest that a careful analysis will be required to draw conclusions about the structural features responsible for blocking H^+ flow through the wild-type voltage sensor. The water within S1–S4 is qualitatively consistent with the concept of high-dielectric aqueous crevices suggested previously (20,61). As illustrated by continuum electrostatic computations using simple geometries (66,67) and an atomic model of *Shaker* (20), a fundamental consequence of such high-dielectric regions is to focus the transmembrane potential (see below).

The transmembrane potential is the driving force responsible for voltage gating. Its influence takes the form of a conformation-dependent contribution to the total free energy of the protein given by Eq. 2. Hence, the shift in the probability of the open and closed states for a given applied transmembrane potential V_{mp} depends on the difference between $\Delta G_{mp}(\mathbf{R}^{(open)};V_{mp})$ and $\Delta G_{mp}(\mathbf{R}^{(closed)};V_{mp})$. Although the coordinates of both the open and closed states, $\mathbf{R}^{(open)}$ and $\mathbf{R}^{(closed)}$, would be required to determine the total gating charge Q_{tot} via the relationship (20,68)

$$Q_{tot}V_{mp} = [\Delta G_{mp}(\mathbf{R}^{(open)};V_{mp}) - \Delta G_{mp}(\mathbf{R}^{(closed)};V_{mp})], \quad (3)$$

the quantity $\phi_{mp}(\mathbf{r})$ obtained from the PB-V Eq. 1 can be used with Eq. 2 to calculate how various residues in the channel are coupled to the transmembrane potential in the open conformational states sampled by the MD simulations. It should be noted that even though the channel configurations in the open state are extracted from MD simulations generated without an applied transmembrane voltage, analysis of those open-channel configurations using the PB-V theory is meaningful. As shown in Fig. 8 *C*, the steepest change in the transmembrane voltage sensed by the charged residues in the S1–S4 bundle occurs mostly over the outer half of the membrane. A similar result was previously obtained using an approximate model of the *Shaker* channel (20). As a comparison, the transmembrane voltage profile across a pure DPPC bilayer (Fig. 8 *C, dotted line*) is shown to vary almost linearly between the peak density of the headgroups, over a distance of ~25–30 Å (47). The aqueous (high-dielectric) regions on the intracellular side, particularly the wide vestibular cavity at the entrance of the pore, as well as the decreased membrane thickness near the channel induced by the multiple interfacial basic residues, are responsible for the extracellularly focused field.

The results of Fig. 8 *C* show that the steepest part of the voltage gradient occurs in the arginine-rich region of the voltage sensor. Accordingly, the transmembrane field is ''focused'', rather than being roughly distributed over the entire thickness of the membrane. Interestingly, the field acting on S1–S4 and the field along the central pore, shown as a solid line in Fig. 8 *C*, are qualitatively similar (43). The latter provides an important reference because it is well established that the membrane voltage acting as a driving force for ion permeation in K^+ channels drops primarily over the length of the narrow selectivity filter (1). Furthermore, the shape of the transmembrane potential along the pore axis of the KcsA K^+ channel has been characterized quantitatively by permeation pore-blocking studies using tetraethylammonium (69). A focusing of the transmembrane field toward the extracellular side, as shown in Fig. 8 *C*, is also consistent with gating-current measurement with *Shaker* channels under conditions of reduced ionic strength (66), experiments using fluorometric probes (70), with tethered charges attached to S4 (71), and mutagenesis data in which an ionic conductance is engineered in the sensor of the *Shaker* channel (72).

Other computational studies concerned with the mechanism of voltage sensing have also described focused electric fields (15,17,73). Previous studies used configurations from MD simulations generated at zero voltage to calculate the total electrostatic potential from all the atoms in the system, whereas we use the configurations in conjunction with the PB-V theory. Despite the apparent similarity, it is important to draw a fundamental distinction. Although the focused field reported in previous simulation studies is interesting (15,17,73), it is not related to the focused voltage gradient that is detected in experimental studies of channel gating (20,61,66,70–72). By virtue of its unique relationship to the free energies $\Delta G_{mp}(\mathbf{R}^{(open)};V_{mp})$ and $\Delta G_{mp}(\mathbf{R}^{(closed)};V_{mp})$ via Eqs. 1 and 2, the potential $\phi_{mp}(\mathbf{r})$ displayed in Fig. 8 *C* governs the effect of the membrane voltage on the relative populations of the open and closed states. For this reason, the results from the PB-V theory, though based on an approximate continuum electrostatic analysis, can be directly linked to experimental observations.

As a consequence of the focused field, the first four arginines along S4 are coupled strongly to the forces driving voltage gating, e.g., if the charges were too far away on the extracellular side, they would not feel a driving force as soon as the membrane is repolarized. Although open/closed equilibrium might remain unaffected, this would certainly slow down kinetic rates. According to the calculations, the field is pulling on each S4 with a force of ~0.75 kcal/mol/Å at 100 mV (up or down, depending on the sign of the voltage). This translates into an incremental gating charge of ~0.3e/Å for each S4. By a crude estimate, the experimentally observed gating charge of 13e would require a movement of ~10 Å for all four S4s in the z-direction, assuming that ϕ_{mp} remains focused, as in the open state. In

comparison, a full translation of S4 over a distance of 25–30 Å would be required if the field was not focused (Fig. 8 C). Although discussing extensively the models of the closed state and their consequences on the gating charge is beyond the scope of this study, these considerations help put the results in the proper context. Furthermore, the idea that the transmembrane field stays focused toward the extracellular side in the closed state is actually supported by previous work. In the model of Chanda et al. (20), the transmembrane field stays focused toward the extracellular side in the closed state due to the opening of a wide aqueous crevice at the intracellular end of the voltage sensor, a view that is also consistent with the sensitivity of the gating charges on ionic strength (66). Recent experimental data that unambiguously constrain the closed state of the *Shaker* channel appear to be consistent with this picture (74,75).

These results are broadly consistent with an atomic view of the structure of phospholipid membranes as a fluid liquid-crystalline phase comprising two hydrophilic headgroup regions surrounding a relatively thin (20–25 Å) central hydrophobic core region unfavorable for polar and charged species (48,76). From this perspective, the lipid bilayer and S1–S4 are well adapted to one another, allowing the stabilization of a complex network of charges throughout the system (Figs. 5 and 8). Importantly, none of the charged residues in S1–S4 is exposed to the central hydrophobic core of the membrane. The two outermost arginines in S4 adopt an interfacial position where they are well hydrated and paired with the lipid phosphate group rather than pointing directly into the nonpolar membrane core as proposed on the basis of the x-ray structure (27). This is consistent with the hydration free energy of arginine side chains, on the order of –60 kcal/mol (77), but contrasts with previous assertions that an isolated S4 would be thermodynamically stable deep in the membrane core by associating with the polar headgroups (73). Consistent with our observations, recent free-energy MD computations show that the cost for transferring a helix with one arginine into the membrane remains prohibitively large, even when pairing with the lipid headgroup (78).

CONCLUSION

The sampling afforded by the simulations discussed here, short on the timescale of the voltage-gating process, is necessarily limited. The moderate-resolution x-ray data introduces additional uncertainties. Nevertheless, the simulations help clarify the physical constraints under which Kv channels operate in the dynamic environment of a hydrated fluid membrane (Fig. 2). From a structural point of view, the modularity of the voltage-sensing domain is directly reflected in the lateral fluctuations relative to the central pore domain (Fig. 3); S4-S4 distances between the voltage sensors of different subunits can vary by as much as ~8 Å. Such large fluctuations suggest that experiments designed to detect

and measure molecular movements upon gating must be interpreted with caution.

No charged residue of the voltage sensor is extensively exposed to the hydrocarbon region of the membrane. The first two arginines along S4 adopt an interfacial position where they interact favorably with water and the lipid headgroups (Fig. 4), whereas the following two arginines interact predominantly with water and E226 in S2. However, extensive pairing of interfacial basic residues with the lipid phosphate group is observed (Figs. 5 and 6). As a consequence, the lipid headgroups are systematically pulled in on the intracellular side and the membrane is thinner near the channel by ~5 Å. As indicated by continuum electrostatic computations, this contributes to the focused transmembrane field, sensed by the charged residues in the voltage sensor (Fig. 8).

Ultimately, whether the charged residues of the voltage sensor will become directly exposed to the nonpolar hydrocarbon core of the membrane during the normal gating operation of the channel is not known, though the simulations show that this is not the case for the activated state of the x-ray structure. The system is organized to offer alternative routes—more palatable than the nonpolar membrane core—to the charged residues (see Figs. 5 and 8). This feature may play a role in enabling the conformational changes (large or small) needed for voltage gating. For example, a translation of S4 accompanied by some rotation around the helix axis (74,75,79) would naturally allow the charged residues to move along a favorable pathway presented by the aqueous crevices lined by countercharges from acidic residues and lipid headgroups (Figs. 5 and 8). Obviously, more work from experiments and computations will be needed to elucidate the nature of the voltage-driven conformational changes of Kv channels.

REFERENCES

1. Hille, B. 2001. Ion Channels of Excitable Membranes, 3rd ed. Sinauer, Sunderland, MA.

2. Bezanilla, F. 2000. The voltage sensor in voltage-dependent ion channels. *Physiol. Rev.* 80:555–592.

3. Seoh, S., D. Sigg, D. Papazian, and F. Bezanilla. 1996. Voltage-sensing residues in the S2 and S4 segments of the *Shaker* K$^+$ channel. *Neuron.* 16:1159–1167.

4. Aggarwal, S., and R. MacKinnon. 1996. Contribution of the S4 segment to gating charge in the *Shaker* K$^+$ channel. *Neuron.* 16:1169–1177.

5. Bezanilla, F., E. Perozo, and E. Stefani. 1994. Gating of *Shaker* K$^+$ channels: II. The components of gating currents and a model of channel activation. *Biophys. J.* 66:1011–1021.

6. Zagotta, W. N., T. Hoshi, and R. W. Aldrich. 1994. *Shaker* potassium channel gating. III: Evaluation of kinetic models for activation. *J. Gen. Physiol.* 103:321–362.

7. Smith-Maxwell, C. J., J. L. Ledwell, and R. W. Aldrich. 1998. Role of the S4 in cooperativity of voltage-dependent potassium channel activation. *J. Gen. Physiol.* 111:399–420.

8. Ledwell, J. L., and R. W. Aldrich. 1999. Mutations in the S4 region isolate the final voltage-dependent cooperative step in potassium channel activation. *J. Gen. Physiol.* 113:389–414.

9. Long, S. B., E. B. Campbell, and R. MacKinnon. 2005. Crystal structure of a mammalian voltage-dependent *Shaker* family K$^+$ channel. *Science.* 309:897–903.

10. Laine, M., M. C. A. Lin, J. P. A. Bannister, W. R. Silverman, A. F. Mock, B. Roux, and D. M. Papazian. 2003. Atomic proximity between S4 segment and pore domain in *Shaker* potassium channels. *Neuron.* 39:467–481.

11. Laine, M., D. M. Papazian, and B. Roux. 2004. Critical assessment of a proposed model of *Shaker. FEBS Lett.* 564:257–263.

12. Murata, Y., H. Iwasaki, M. Sasaki, K. Inaba, and Y. Okamura. 2005. Phosphoinositide phosphatase activity coupled to an intrinsic voltage sensor. *Nature.* 435:1239–1243.

13. Sasaki, M., M. Takagi, and Y. Okamura. 2006. A voltage sensor-domain protein is a voltage-gated proton channel. *Science.* 312:589–592.

14. Ramsey, I. S., M. M. Moran, J. A. Chong, and D. E. Clapham. 2006. A voltage-gated proton-selective channel lacking the pore domain. *Nature.* 440:1213–1216.

15. Treptow, W., and M. Tarek. 2006. Environment of the gating charges in the Kv1.2 *Shaker* potassium channel. *Biophys. J.* 90:L64–L66.

16. Sands, Z. A., A. Grottesi, and M. S. Sansom. 2006. The intrinsic flexibility of the Kv voltage sensor and its implications for channel gating. *Biophys. J.* 90:1598–1606.

17. Freites, J. A., D. J. Tobias, and S. H. White. 2006. A voltage-sensor water pore. *Biophys. J.* 91:L90–L92.

18. Jiang, Y., A. Lee, J. Chen, V. Ruta, M. Cadene, B. Chait, and R. MacKinnon. 2003. X-ray structure of a voltage-dependent K$^+$ channel. *Nature.* 423:33–41.

19. Jiang, Y., A. Lee, J. Chen, M. Cadene, B. T. Chait, and R. MacKinnon. 2002. Crystal structure and mechanism of a calcium-gated potassium channel. *Nature.* 417:515–522.

20. Chanda, B., O. K. Asamoah, R. Blunck, B. Roux, and F. Bezanilla. 2005. Gating charge displacement in voltage-gated ion channels involves limited transmembrane movement. *Nature.* 436:852–856.

21. Silverman, W. R., B. Roux, and D. M. Papazian. 2003. Structural basis of two-stage voltage-dependent activation in K$^+$ channels. *Proc. Natl. Acad. Sci. USA.* 100:2935–2940.

22. Gonzalez, C., E. Rosenman, F. Bezanilla, O. Alvarez, and R. Latorre. 2001. Periodic perturbations in *Shaker* K$^+$ channel gating kinetics by deletions in the S3–S4 linker. *Proc. Natl. Acad. Sci. USA.* 98:9617–9623.

23. Monks, S. A., D. J. Needleman, and C. Miller. 1999. Helical structure and packing orientation of the S2 segment in the *Shaker* K$^+$ channel. *J. Gen. Physiol.* 113:415–423.

24. Hong, K. H., and C. Miller. 2000. The lipid-protein interface of a *Shaker* K$^+$ channel. *J. Gen. Physiol.* 115:51–58.

25. Li-Smerin, Y., D. H. Hackos, and K. J. Swartz. 2000. α-helical structural elements within the voltage-sensing domains of a K$^+$ channel. *J. Gen. Physiol.* 115:33–50.

26. Li-Smerin, Y., and K. J. Swartz. 2001. Helical structure of the COOH terminus of S3 and its contribution to the gating modifier toxin receptor in voltage-gated ion channels. *J. Gen. Physiol.* 117:205–218.

27. Long, S. B., E. B. Campbell, and R. MacKinnon. 2005. Voltage sensor of Kv1.2: structural basis of electromechanical coupling. *Science.* 309:903–908.

28. Bower, M. J., F. E. Cohen, and R. L. Dunbrack, Jr. 1997. Prediction of protein side-chain rotamers from a backbone-dependent rotamer library: a new homology modeling tool. *J. Mol. Biol.* 267:1268–1282.

29. Dunbrack, R. L., and M. Karplus. 1993. Backbone-dependent rotamer library for proteins. Application to side-chain prediction. *J. Mol. Biol.* 230:543–574.

30. Woolf, T. B., and B. Roux. 1994. Molecular dynamics simulation of the gramicidin channel in a phospholipid bilayer. *Proc. Natl. Acad. Sci. USA.* 91:11631–11635.

31. Bernèche, S., M. Nina, and B. Roux. 1998. Molecular dynamics simulation of melittin in a dimyristoylphosphatidylcholine bilayer membrane. *Biophys. J.* 75:1603–1618.

32. Bernèche, S., and B. Roux. 2000. Molecular dynamics of the KcsA K$^+$ channel in a bilayer membrane. *Biophys. J.* 78:2900–2917.

33. Brooks, B. R., R. E. Bruccoleri, B. D. Olafson, D. J. States, S. Swaminathan, and M. Karplus. 1983. CHARMM: a program for macromolecular energy minimization and dynamics calculations. *J. Comput. Chem.* 4:187–217.

34. MacKerell, A. D. J., D. Bashford, M. Bellot, R. L. Dunbrack, J. D. Evanseck, M. J. Field, S. Fischer, J. Gao, H. Guo, D. J.-M. S. Ha, L. Kuchnir, K. Kuczera, F. T. K. Lau, C. Mattos, S. Michnick, T. Ngo, D. T. Nguyen, B. Prodhom, W. E. Reiher III, B. Roux, M. Schlenkrich, J. Smith, R. Stote, J. Straub, M. Watanabe, J. Wiorkiewicz-Kuczera, and M. Karplus. 1998. All-atom empirical potential for molecular modeling and dynamics studies of proteins. *J. Phys. Chem. B.* 102: 3586–3616.

35. Schlenkrich, M. J., J. Brickmann, A. D. J. MacKerell, and M. Karplus. 1996. An empirical potential energy function for phospholipids: criteria for parameters optimization and applications. *In* Biological Membranes. A Molecular Perspective from Computation and Experiment. Birkhauser, Boston. 31–81.

36. Jorgensen, W. L., J. Chandrasekhar, J. D. Madura, R. W. Impey, and M. L. Klein. 1983. Comparison of simple potential functions for simulating liquid water. *J. Chem. Phys.* 79:926–935.

37. Beglov, D., and B. Roux. 1994. Finite representation of an infinite bulk system: solvent boundary potential for computer simulations. *J. Chem. Phys.* 100:9050–9063.

38. Essmann, U., L. Perera, M. Berkowitz, T. Darden, H. Lee, and L. Pedersen. 1995. A smooth particle mesh Ewald method. *J. Chem. Phys.* 103:8577–8593.

39. Feller, S., Y. Zhang, R. Pastor, and B. Brooks. 1995. Constant pressure molecular dynamics simulation: the Langevin piston method. *J. Chem. Phys.* 103:4613–4621.

40. Chapman, D. 1975. Fluidity and phase transitions of cell membranes. *Biomembranes.* 7:1–9.

41. Ryckaert, J., G. Ciccotti, and H. Berendsen. 1977. Numerical integration of the Cartesian equation of motions of a system with constraints: molecular dynamics of *n*-alkanes. *J. Comput. Phys.* 23: 327–341.

42. Roux, B. 1997. The influence of the membrane potential on the free energy of an intrinsic protein. *Biophys. J.* 73:2980–2989.

43. Roux, B., S. Bernèche, and W. Im. 2000. Ion channels, permeation and electrostatics: insight into the function of KcsA. *Biochemistry.* 39: 13295–13306.

44. Tiwari-Woodruff, S. K., C. T. Schulteis, A. F. Mock, and D. M. Papazian. 1997. Electrostatic interactions between transmembrane segments mediate folding of *Shaker* K$^+$ channel subunits. *Biophys. J.* 72:1489–1500.

45. Tiwari-Woodruff, S. K., M. A. Lin, C. T. Schulteis, and D. M. Papazian. 2000. Voltage-dependent structural interactions in the *Shaker* K$^+$ channel. *J. Gen. Physiol.* 115:123–138.

46. Papazian, D. M., W. R. Silverman, M.-C. A. Lin, S. K. Tiwari-Woodruff, and C. Y. Tang. 2002. Structural organization of the voltage sensor in voltage-dependent potassium channels. *In* Ion Channels: From Atomic Resolution Physiology to Functional Genomics. Novartis Foundation Symposia Series. G. Bock and J. A. Goode, editors. Wiley Interscience, Hoboken, NJ. 178–190.

47. Sachs, J. N., P. S. Crozier, and T. B. Woolf. 2004. Atomistic simulations of biologically realistic transmembrane potential gradients. *J. Chem. Phys.* 121:10847–10851.

48. Klauda, J. B., B. R. Brooks, and R. W. Pastor. 2006. Dynamical motions of lipids and a finite size effect in simulations of bilayers. *J. Chem. Phys.* 125:144710.

49. Cha, A., G. Snyder, P. Selvin, and F. Bezanilla. 1999. Atomic scale movement of the voltage-sensing region in a potassium channel measured via spectroscopy. *Nature.* 402:809–813.

50. Blaustein, R., P. Cole, C. Williams, and C. Miller. 2000. Tethered blockers as molecular ''tape measures'' for a voltage-gated K$^+$ channel. *Nat. Struct. Biol.* 7:309–311.

51. Jiang, Y., V. Ruta, J. Chen, A. Lee, and R. MacKinnon. 2003. The principle of gating charge movement in a voltage-dependent K$^+$ channel. *Nature.* 423:42–48.

52. Selvin, P. R. 2002. Principles and biophysical applications of lanthanide-based probes. *Annu. Rev. Biophys. Biomol. Struct.* 31:275–302.

53. Elinder, F., P. Arhem, and H. P. Larsson. 2001. Localization of the extracellular end of the voltage sensor S4 in a potassium channel. *Biophys. J.* 80:1802–1809.

54. Gandhi, C., E. Clark, E. Loots, A. Pralle, and E. Isacoff. 2003. The orientation and molecular movement of a K$^+$ channel voltage-sensing domain. *Neuron.* 40:515–525.

55. Soler-Llavina, G. J., T. H. Chang, and K. J. Swartz. 2006. Functional interactions at the interface between voltage-sensing and pore domains in the *Shaker* K$_v$ channel. *Neuron.* 52:623–634.

56. Guy, H. R., and P. Seetharamulu. 1986. Molecular model of the action potential sodium channel. *Proc. Natl. Acad. Sci. USA.* 83:508–512.

57. Catterall, W. A. 1988. Structure and function of voltage-sensitive ion channels. *Science.* 242:50–61.

58. Schmidt, D., Q. X. Jiang, and R. MacKinnon. 2006. Phospholipids and the origin of cationic gating charges in voltage sensors. *Nature.* 444:775–779.

59. Deol, S. S., C. Domene, P. J. Bond, and M. S. Sansom. 2006. Anionic phospholipid interactions with the potassium channel KcsA: simulation studies. *Biophys. J.* 90:822–830.

60. Mishra, V. K., M. N. Palgunachari, J. P. Segrest, and G. M. Anantharamaiah. 1994. Interactions of synthetic peptide analogs of the class A amphipathic helix with lipids. Evidence for the snorkel hypothesis. *J. Biol. Chem.* 269:7185–7191.

61. Starace, D., and F. Bezanilla. 2004. A proton pore in a potassium channel voltage sensor reveals a focused electric field. *Nature.* 427:548–553.

62. Tombola, F., M. M. Pathak, and E. Y. Isacoff. 2005. Voltage-sensing arginines in a potassium channel permeate and occlude cation-selective pores. *Neuron.* 45:379–388.

63. Pomes, R., and B. Roux. 1996. Structure and dynamics of a proton wire: a theoretical study of H$^+$ translocation along the single-file water chain in the gramicidin A channel. *Biophys. J.* 71:19–39.

64. Chakrabarti, N., E. Tajkhorshid, B. Roux, and R. Pomes. 2004. Molecular basis of proton blockage in aquaporins. *Structure.* 12:65–74.

65. Ilan, B., E. Tajkhorshid, K. Schulten, and G. A. Voth. 2004. The mechanism of proton exclusion in aquaporin channels. *Proteins.* 55:223–228.

66. Islas, L. D., and F. J. Sigworth. 2001. Electrostatics and the gating pore of *Shaker* potassium channels. *J. Gen. Physiol.* 117:69–89.

67. Grabe, M., H. Lecar, Y. N. Jan, and L. Y. Jan. 2004. A quantitative assessment of models for voltage-dependent gating of ion channels. *Proc. Natl. Acad. Sci. USA.* 101:17640–17645.

68. Sigworth, F. J. 1993. Voltage gating of ion channels. *Quat. Rev. Biophys.* 27:1–40.

69. Kutluay, E., B. Roux, and L. Heginbotham. 2005. Rapid intracellular TEA block of the KcsA potassium channel. *Biophys. J.* 88:1018–1029.

70. Asamoah, O. K., J. P. Wuskell, L. M. Loew, and F. Bezanilla. 2003. A fluorometric approach to local electric field measurements in a voltage-gated ion channel. *Neuron.* 37:85–97.

71. Ahern, C. A., and R. Horn. 2005. Focused electric field across the voltage sensor of potassium channels. *Neuron.* 48:25–29.

72. Tombola, F., M. M. Pathak, P. Gorostiza, and E. Y. Isacoff. 2006. The twisted ion-permeation pathway of a resting voltage-sensing domain. *Nature.*

73. Freites, J. A., D. J. Tobias, G. von Heijne, and S. H. White. 2005. Interface connections of a transmembrane voltage sensor. *Proc. Natl. Acad. Sci. USA.* 102:15059–15064.

74. Campos, F. V., B. Chanda, B. Roux, and F. Bezanilla. 2007. Two atomic constraints unambiguously position the S4 segment relative to S1 and S2 segments in the closed state of *Shaker* K channel. *Proc. Natl. Acad. Sci. USA.* 104:7904–7909.

75. Pathak, M. M., V. Yarov-Yarovoy, G. Agarwal, B. Roux, P. Barth, S. Kohout, F. Tombola, and E. Y. Isacoff. 2007. Closing in on the resting state of the *Shaker* K$^+$ channel. *Neuron.* In press.

76. Wiener, M. C., and S. H. White. 1992. Structure of a fluid dioleoylphosphatidylcholine bilayer determined by joint refinement of x-ray and neutron diffraction data. II. Distribution and packing of terminal methyl groups. *Biophys. J.* 61:428–433.

77. Deng, Y., and B. Roux. 2004. Hydration of amino acid side chains: non-polar and electrostatic contributions calculated from staged molecular dynamics free energy simulations with explicit water molecules. *J. Phys. Chem. B.* 108:16567–16576.

78. Dorairaj, S. J., and T. W. Allen. 2007. The energetics of arginine-membrane interactions. *Proc. Natl. Acad. Sci. USA.* 104:4943–4948.

79. Yarov-Yarovoy, V., D. Baker, and W. A. Catterall. 2006. Voltage sensor conformations in the open and closed states in ROSETTA structural models of K$^+$ channels. *Proc. Natl. Acad. Sci. USA.* 103:7292–7297.

New and Notable

The Last Few Frames of the Voltage-Gating Movie

Fred J. Sigworth
Department of Cellular and Molecular Physiology, Yale University, New Haven, Connecticut

In the voltage sensor domain (VSD) of a voltage-gated channel, electrical charge is driven from the intracellular to the extracellular surface of a membrane as conformational changes occur and the channel gates are opened. This charge displacement, which in voltage-gated potassium channels occurs in ~1 ms, is measured as a "gating current."

A few years ago Sigg et al. (1) reported a component of the charge displacement that occurs in ~10 μs, two orders-of-magnitude faster than the ordinary gating current. This fast charge movement (I call it the "loose charge") was best modeled as a tethered diffusion, implying that the VSD's resting "state" is actually a very flexible conformation that allows protein charges to move quite freely. The loose charge, which makes a substantial contribution to the membrane capacitance when Shaker voltage-gated channels are expressed in *Xenopus* oocytes, is entirely absent in uninjected oocytes. From this, one concludes that there is something very special about voltage-gated channels, that among all the membrane proteins in oocytes, only they have such a large mobile charge. Now, in this issue of *Biophysical Journal*, a molecular dynamics study by Jogini and Roux (2) gives us a view of the substantial rocking and rolling of VSDs and their gating charge that makes the loose charge movement look quite tame.

In recent years, workers in Rod MacKinnon's laboratory have solved x-ray structures of two voltage-gated potassium channels. The first structure, of the archaebacterial channel KvAP, caused much consternation as it implied that, in the process of activation, the voltage sensor "paddles" (each a helical hairpin formed from the S3 and S4 VSD helices) would traverse the membrane while largely exposed to the hydrophobic membrane interior. It is now generally accepted that, in the KvAP crystals, the VSDs were held in an unnatural conformation. This conclusion is bolstered by the second x-ray structure, of the rat brain channel Kv1.2. The Kv1.2 crystal form resembles a stack of lipid-bilayer membranes, and presents a view of the VSDs that agrees much better with the many other experimental results that have accumulated in the past decade. This structure by Long et al. (3) shows a channel whose voltage sensors are fully activated (or maybe forced into the inactivated state as is seen after a long depolarization): we know this because the first four arginines in the S4 helix, the ones that carry the gating charge, are all exposed to the extracellular side of the membrane.

Now all that is needed is to extend this still picture—the Kv1.2 structure—into a movie that will illustrate the remarkable conformational change involved in voltage sensor activation. The VSD is not large; it is a membrane-embedded four-helix bundle, but somehow it rearranges itself in response to a voltage change to transport ~3.5 e_0 of charge from one side of the membrane to the other. The Kv1.2 structure provides a frozen frame near the end; but can we reconstruct the rest of the movie?

In molecular dynamics (MD) simulations, atoms are modeled as charged van der Waals spheres, and bonds are modeled as springs. This classical representation of what are actually fuzzy, polarizable, quantum mechanical atoms and bonds is surprisingly successful in predicting free energies and illuminating protein structural changes. In the analysis of the ion permeation process, MD techniques have resulted in a remarkably good prediction of the current-voltage curve of a potassium channel (4), and have shown how ion selectivity can arise simply from the number and type of ion-coordinating ligands (5).

Since MD can model an ion moving through a channel's selectivity filter, why not use MD to show us how the charged residues move as the Kv1.2 channel activates? There are two problems. First, a good idea of the reaction coordinates is required. For ion permeation, the reaction coordinates can only be the z position of each permeating ion. The VSD, on the other hand, has very many potentially relevant degrees of freedom, and without a crystal structure of a deactivated VSD, one does not know where to place the starting point of the reaction pathway. Second, there is the issue of the timescale accessible to MD, which is considerably less than 1 μs. Because of this limitation there is little hope of a brute force approach involving the simulation of the entire activation or deactivation process, which at best might be coaxed to occur in some tens of microseconds.

In the meantime, however, there is considerable value in simply looking at the motions and energetics of Kv1.2 in a lipid bilayer membrane, with its voltage sensors remaining activated as they were in the crystal structure. Jogini and Roux studied a large model system—some 77,000 atoms—that included a stripped-down Kv1.2 tetrameric channel, a lipid bilayer, and a 100 mM KCl solution. The channel subunits were truncated to include little more than the transmembrane portion; this is a simplification that is justified from experimental observations of normal channel activity expressed from similarly truncated cRNA sequences. Jogini and Roux's work is the latest of several recent MD simulations of voltage-sensing proteins in lipid bilayer membranes. Sands and Sansom (6) have simulated the isolated voltage sensor domain of KvAP, as have Freites

et al. (7). Treptow and Tarek (8) have constructed a large system encompassing the entire Kv1.2 channel including its cytoplasmic T1 domains.

It is known from a wide variety of experiments that the charge translocation involved in the voltage-sensing process involves a movement of S4 arginines through a "focused" electric field, in which the transmembrane potential difference drops across a short distance. The focusing allows relatively small molecular motions to produce large charge movements and high voltage sensitivity. It is also known that salt bridges between acidic residues in S2 and S3 serve to stabilize some of the S4 charges. These aspects of VSD dogma are now clarified and extended by the MD results. Very recently, it was demonstrated that the presence of lipid phosphodiester groups is necessary for the proper functioning of a voltage-gated channel (9). The MD results now provide a tantalizing explanation for this phenomenon as well.

FOCUSED ELECTRIC FIELD

All of the recent simulation studies show extracellular and intracellular water-filled crevices that together form an hourglass-shaped aqueous region. Waters do not penetrate the central region, over which the transmembrane potential drops most steeply. However, to estimate quantitatively the electric field component that changes with membrane potential is a nontrivial undertaking; to date this been accomplished only in a heroic simulation of two lipid bilayer membranes by Sachs et al. (10). Jogini and Roux provide the next best thing, an approximate calculation using continuum electrostatics and a linear theory based on the Poisson-Boltzmann equation and the Ramo-Shockley theorem (11). Because the model is linear, they can invoke superposition to ignore the protein's fixed charges and simply calculate the contribution to the potential at a given atom due to the transmembrane potential difference. The resulting potential profile has a maximum steepness approximately three times that obtained from a constant electric field.

STABILIZATION OF ARGININES

Laying to rest the fears raised by the original "paddle model," all the MD studies show that the S4 arginine side chains are not found in the nonpolar membrane interior, but are hydrated and paired with other charged groups. Acidic residues on the S2 and S3 helices, and also an aspartate on S5, are found in association with S4 arginines. And of particular interest is the observation that the two outermost arginines are found to be paired with one or more lipid phosphodiester groups. This provides a very promising explanation for the phosphodiester requirement for function of the KvAP channel. Perhaps these interactions are necessary to stabilize the activated states of the voltage sensors, allowing the channels to open. Jogini and Roux show further that many other basic residues located near the level of the membrane-water interface form salt bridges with lipid phosphates. The result is a net thinning of the membrane by ~ 5 Å near the channel protein, which has a further effect in focusing the electric field.

MOBILITY OF VOLTAGE SENSOR DOMAINS

In the Kv2.1 structure the VSDs are four distinct modules that are arrayed around the periphery of the pore-containing channel core. Each VSD interacts with the core through an α-helix (the S4-S5 linker), through which its activation is coupled to channel opening; the remaining nonbonded connections to the core are not rigid, as only a third of the lateral surface area of a VSD abuts the core. It is thus not surprising that the VSDs are seen to swing from side to side through distances of 5–6 Å and, given enough time, are likely to sample very large displacements. Such motions could explain experimental evidence for the ability of residues to crosslink between VSDs; they also imply that spectroscopic measurements of distances between VSDs need to be interpreted with caution.

There are considerable vertical motions in the voltage sensor as well, with the z-coordinates of the arginine guanidinium moieties fluctuating by ~ 2 Å rms. In view of the focused electric field, which causes $\sim 5\%$ of the transmembrane potential to fall over each angstrom of z displacement, a correlated movement of the four arginines could produce a transmembrane charge fluctuation of ~ 0.5 e_0 rms. This charge movement alone could result in a doubling of the membrane capacitance at high channel densities. Given a more damped motion, it would readily account for the size of the "loose charge" movement, ~ 1.0 e_0, that was seen by Sigg et al. (1).

It should, however, be kept in mind that there are two differences between the loose charge and the z motions observed by Jogini and Roux. First, the loose charge moves on a timescale of 10 μs, which is very long compared to the nanosecond-scale fluctuations observed in the MD simulations. In electrical experiments, nanosecond-scale charge movements would be indistinguishable from an increment in membrane capacitance. Second, Sigg et al. observed the loose charge only in the resting state of the voltage sensors; in the activated state, the loose charge was not visible. These differences can be reconciled if the nanosecond-scale charge movements are similar in both resting and activated states, while an additional slower charge movement occurs only in the resting state. Nevertheless, the picture of VSDs provided by Jogini and Roux is one of a very mobile voltage-sensor domain, with a focused electric field that converts small physical motions into large transmembrane charge movements. It is no wonder that voltage-gated channels incorporating these domains show such large charge movements compared to other membrane proteins.

REFERENCES

1. Sigg, D., F. Bezanilla, and E. Stefani. 2003. Fast gating in the *Shaker* K$^+$ channel and

the energy landscape of activation. *Proc. Natl. Acad. Sci. USA.* 100:7611–7615.

2. Jogini, V., and B. Roux. 2007. Dynamics of the Kv1.2 voltage-gated K^+ channel in a membrane environment. *Biophys. J.*

3. Long, S. B., E. B. Campbell, and R. Mackinnon. 2005. Crystal structure of a mammalian voltage-dependent *Shaker* family K^+ channel. *Science.* 309:897–903.

4. Berneche, S., and B. Roux. 2003. A microscopic view of ion conduction through the K^+ channel. *Proc. Natl. Acad. Sci. USA.* 100:8644–8648.

5. Noskov, S. Y., and B. Roux. 2007. Importance of hydration and dynamics on the selectivity of the KcsA and NaK channels. *J. Gen. Physiol.* 129:135–143.

6. Sands, Z. A., and M. S. Sansom. 2007. How does a voltage sensor interact with a lipid bilayer? Simulations of a potassium channel domain. *Structure.* 15:235–244.

7. Freites, J. A., D. J. Tobias, and S. H. White. 2006. A voltage-sensor water pore. *Biophys. J.* 91:L90–L92.

8. Treptow, W., and M. Tarek. 2006. Environment of the gating charges in the Kv1.2 *Shaker* potassium channel. *Biophys. J.* 90:L64–L66.

9. Schmidt, D., Q. X. Jiang, and R. MacKinnon. 2006. Phospholipids and the origin of cationic gating charges in voltage sensors. *Nature.* 444:775–779.

10. Sachs, J. N., P. S. Crozier, and T. B. Woolf. 2004. Atomistic simulations of biologically realistic transmembrane potential gradients. *J. Chem. Phys.* 121:10847–10851.

11. Nonner, W., A. Peyser, D. Gillespie, and B. Eisenberg. 2004. Relating microscopic charge movement to macroscopic currents: the Ramo-Shockley theorem applied to ion channels. *Biophys. J.* 87:3716–3722.